Journal of Solid State Chemistry **153,** 48–54 (2000)
doi:10.1006/jssc.2000.8738, available online at http://www.idealibrary.com on IDEAL®

Crystal Structure of $BiZn_2PO_6$. Filiation between Related Compounds

El mostafa Ketatni,*[,1] Bouchaib Mernari,* Francis Abraham,† and Olivier Mentre†[,2]

*Laboratoire de Chimie Coordination et Analytique, Faculté des Sciences, Université Chouaïb Doukkali, B.P. 20, El Jadida, Morocco; and †Laboratoire de Cristallochimie et Physicochimie du Solide UPRES A, CNRS 8012 ENSCL, Université des Sciences et Technologies de Lille, B.P. 108, 59652 Villeneuve d'Ascq Cedex, France

Received January 5, 2000; in revised form March 27, 2000; accepted April 7, 2000; published online June 27, 2000

The $BiZn_2PO_6$ room-temperature crystal structure was determined from powder X-ray data using the Rietveld method. This compound crystallizes in space group *Pnma*, with $Z = 4$, $a = 11.897(2)$ Å, $b = 5.277(1)$ Å, $c = 7.819(2)$ Å. The structure contains ZnO_5 square pyramids associated by edge in dimers which are connected by corners to form infinite independent $[ZnO_3^{4-}]_\infty$ zigzag double chains. The interconnection is achieved by PO_4^{3-} tetrahedra creating six-sided tunnels parallel to the *b* axis containing Bi^{3+} cations. An intensive discussion about the structural filiation between the different members of the BiM_2XO_6 series (M = Mg, Ca, Cu, Cd, Pb; X = P, V, As) is given. A thermal investigation showed that $BiZn_2PO_6$ undergoes a *P*-to-*B* phase transition at about 325°C while this isostructural $BiCu_2PO_6$ remains structurally unchanged until 750°C. © 2000 Academic Press

Key Words: bismuth phosphate; phase transition.

INTRODUCTION

The several compounds found with the formula $Bi^{III}M_2^{II}XO_6$ (X = As, P, V; M = Mg, Ca, Cu, Cd, Pb) (1–8) are currently intensively studied for the network ability to adopt different cations without drastic changes. As an example, two new compounds, $BiCd_2VO_6$ and $BiCu_2AsO_6$, were very recently reported (9, 10). From a structural point of view, the materials remain closely related independently of the X/M combination. Therefore, slight changes allow a primary classification in several subgroups. This distinction is based on the adopted space group of the orthorhombic cell, i.e., *Pnma*, *Bbmm*, and $Bb2_1m$, using the $a \approx 11.5$ Å, $b \approx 5.7$ Å, $c \approx 7.8$ Å unit cell orientation. The common feature for all the series is the tridimensional framework built up from covalently bound $(BiO_2)^-$ infinite chains and XO_4^{3-} tetrahedra with charge balance provided by interspersed M^{2+} cations. The adopted space group essentially results from the XO_4 tilt angle leading to strong distortion of the MO_x polyhedron (11). So far, this aspect of the crystal structure was not clearly approached but still appears necessary for a good comprehension of the lattice changes arising in the different materials. In that frame, we studied the already reported $BiZn_2PO_6$ compound that remains structurally uncharacterized in previous works. Actually, it was reported to adopt a monoclinic unit cell (2) while we unambiguously refined its crystal structure with the *Pnma* space group. Furthermore, the $BiMg_2PO_6$ compound was very recently reported to undergo a transition from *B* to *P* between 300 and 350 K in contrast with its previous *Bbmn* space group assignment at room temperature (12). This result let us envisage a similar transition *P* to *B* at high temperature for $BiZn_2PO_6$ and $BiCu_2PO_6$, reinforced by the weak intensities of the no-*B* reflections (*hkl*, $h + l = 2n + 1$) for the former. This paper is devoted to the $BiZn_2PO_6$ room-temperature crystal structure refinement from powder XRD. High-temperature X-ray diffraction was also investigated. The description and comparison with other BiM_2XO_6 materials are given in terms of MO_x polyhedron linkage. The Bi^{3+} $6s^2$ lone pair localization is also reported in this work.

EXPERIMENTAL

The powder sample corresponding to the formula $BiZn_2PO_6$ was synthesized by solid-state reaction of Bi_2O_3 (Aldrich, 99.9%), ZnO (Cerac, 99.9%), and $(NH_4)_2HPO_4$ (Fluka, purity > 99%). A stoichiometric mixture of the reactants was thoroughly ground in an agate mortar and then successively preheated at 300°C and 500°C for 12 h to decompose $(NH_4)_2HPO_4$. The reaction was complete after annealing at 770°C for 4 days in an alumina crucible in air. An intermediate regrinding was necessary to obtain pure material. Our attempts to prepare the analogous vanadate compound systematically failed, leading to a mixture of unidentified phases and a $BiVO_4$-related compound. Identification was done by powder X-ray diffraction using

[1]Permanent address: Université Cadi Ayyad, Faculté des Sciences et Techniques, Department de Chimie et Environnement, B.P. 523, Beni Mellal, Morocco.

[2]To whom correspondence should be addressed. E-mail: mentre@ensc-lille.fr.

0022-4596/00 $35.00

a Siemens D5000 powder diffractometer equipped with a diffracted-beam graphite monochromator and Cu$K\alpha$ radiation. The presented high-temperature diagrams were collected using a Guinier–Lenné diffraction system, Ni-filtered Cu$K\alpha$. The thermal analysis was performed with a LINSEIS L62 DT analyzer and a DSC 141 SETARAM.

STRUCTURE SOLUTION AND DESCRIPTION

Data Collection and Structure Refinement

The powder X-ray diffraction data used for the structure determination were collected at room temperature from 10 to 123° (2θ) using a 0.02° step size with a count time of 40 seconds. Accurate orthorhombic lattice parameters were refined from the 10–60° range, 2θ XRD pattern, using the program Profile from the Siemens Diffrac/AT package (13). The chosen unit cell orientation for the discussion to come is $a = 11.897(2)$ Å, $b = 5.277(1)$ Å, $c = 7.189(2)$ Å, $F(30) = 45(0.010, 67)$ (14), after least-squares refinement. These parameters are significant with regard to Rietveld refinement results for which standard deviations are underevaluated. No evidence of the monoclinic symmetry reported in (2) was observed. Among the peak list, weak primitive reflections are clearly present while systematic absences are in favor of the *Pnma* space group adopted by $BiCu_2PO_6$. The existence of weak reflections with $h0l$, $h + l = 2n + 1$ refute the *Pbnm* space group reported for $BiPb_2PO_6$ (6) (in our orientation). The complete diffractogram was treated with the Rietveld method using the Fullprof 98 package (15). The pseudo-Voigt profile shape function was first tried but did not satisfactorily match the diagram. We subsequently used the Pearson function that allows an excellent profile fitting. Atoms positions were introduced within the process from the $BiCu_2PO_6$ model. The refinement satisfactorily converged. In the final cycles, anisotropic displacement was considered for the unique bismuth atom, enabling a sensitive refinement improvement. No significant residual electronic density appeared on the last difference Fourier maps. A full-matrix refinement with 44 refined parameters was performed, yielding final $R_p = 12.4\%$, $R_{wp} = 15.5\%$, $R_{Bragg} = 5.64\%$, $R_F = 3.80\%$, and $\chi^2 = 4.49$. The agreement between observed and calculated diffraction patterns is shown in Fig. 1. Details of the data collection and refinement are summarized in Table 1. The final atomic parameters and thermal parameters are reported in Table 2.

Lone Pair Localization

Selected distances and bond angles are given in Table 3. As a constancy in all of the BiM_2XO_6 series members, the structure of $BiZn_2PO_6$ is formed of infinite BiO_2^- chains running parallel to the b axis. Thus Bi is covalently bonded to four O(1) atoms, $2 \times 2.29(1)$ Å and $2 \times 2.33(1)$ Å, forming a BiO_4 square pyramid. Each O(1) atom bonds two Bi atoms, leading to zigzag chains (Fig. 2). The calculated distances are significantly longer than in $BiMg_2PO_6$ or $BiCa_2VO_6$ (Bi–O(1) ≈ 2.20 Å). In contrast, $BiCu_2PO_6$ shows a greater discrepancy between the two pairs of distances with Bi–O(1) of 2.189(6) and 2.361(6) Å alternating along the b axis. The $BiO(1)_4$ polyhedron is to be completed with three longer distances close to 3 Å on the opposite side as shown in Fig. 2. Such an environment is commonly found for $6s^2$ lone pair (Lp)-possessing cations. In these cations the partial hybridization of full ns^2 long pair with its np^0 empty shell is known as the lone pair effect that forms a supplementary entity, two electrons loaded, filling the volume of about one F^- or O^{2-} anion (16). Under the influence of the local electric field, E_{loc} at the cation i center, the lone pair is displaced by an amount d_i which can be deduced by the relation $\mu_i = qd_i = \alpha_i E_{loc}$, where q is the electric charge of the lone pair, namely -2. μ_i is the dipolar momentum of the ion-Lp dipole and α_i its electronic polarizability. Assuming knowledge of the latter, Verbaere *et al.* proposed a method to determine the displacement of the ns^2 lone pair from its cation core (17). The local electric field is calculated from electrostatic interactions in the whole crystal using the Ewald's method (18). This formula was recently computerized in the program HYBRIDE at the Laboratorie de Cristallochimie du Solide, University Paris IV (19). The used bismuth polarizability value is 6.12 Å^3 (20). The valence of each element was used for the local charge. The calculation yields the results given in Table 3.

Crystal Structure Description

The PO_4^{3-} groups are distorted with two short distances (1.43 and 1.44 Å) with O(4) and O(3) atoms shared with one ZnO_5 polyhedron, $Zn(1)O_5$ and $Zn(2)O_5$ respectively, and two longer distances (1.56 Å) with O(2) atoms involved in the coordination of both Zn(1) and Zn(2) atoms. The short lengths with regard to As–O and V–O bonds are partially responsible for the drastic lattice parameters evolution between the $BiMg_2XO_6$ members. Table 4 reports the lattice parameters versus the M^{2+} cationic size for several BiM_2XO_6 compounds. PO_4 tetrahedra and $[BiO_2]^-$ chains are independent while PO_4^{3-} corners participate in the Zn^{2+} coordinations, i.e., ZnO_5 square pyramids. At that point, we must recall that in $BiCu_2PO_6$ (11) material that Bi–O(4) distance is significantly shorter than in most of the other cases, 2.49 Å long, leading to an additional strong bond between phosphates and chains as explained in the discussion to come.

As we already mentioned, infinite columns formed by the MO_x polyhedron linkage were rarely discussed in previous works but M^{2+} cations were, most of the time, considered as hosts of the BiO_2 and PO_4 framework. Nevertheless, this description seems necessary for a good comparison of the

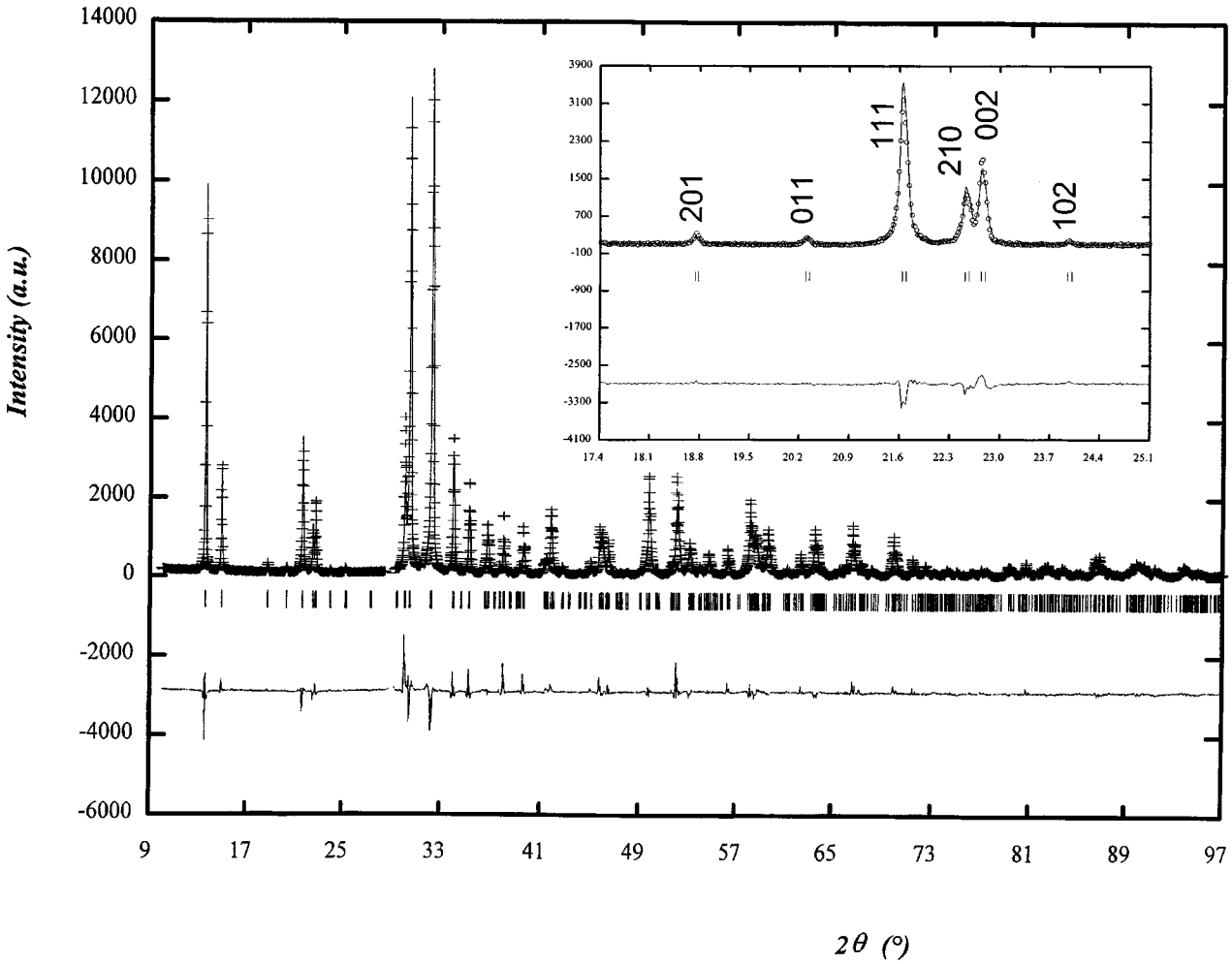

FIG. 1. Observed, calculated, and difference plots for $BiZn_2PO_6$. The inset shows weak primitive reflections.

different materials of this rich series. A large part of the discussion will be devoted to that point. In $BiZn_2PO_6$, Zn^{2+} cations occupy the center of a square pyramid formed by two O(1), two O(2), and one O(4) or O(3) atoms for Zn(1) and Zn(2) respectively. Two pyramids share their O(2)–O(2) edge and give rise to dimers with an intradimeric Zn(1)–Zn(2) distance of 3.05 Å. Along the *b* axis, each dimer connects two others by its four O(1) corners (Fig. 3), and so the ZnO_5 entities form infinite $[ZnO_3^{4-}]_\infty$ zigzag double columns running along the *b* axis. The resulting short and long Zn–Zn interdimer distances are respectively 3.52 and 4.56 Å. The interdimer cohesion is consolidated by bidentate phosphate groups that connect two consecutive dimers by O(2) corners. The independent columns are connected by phosphate groups and create six-sided tunnels in which the $[BiO_2]^-$ chains are running. Figure 4 presents a projection along [010] enabling us to distinguish the tunnel sections and their Bi hosts.

DISCUSSION—STRUCTURAL FILIATION

As observed in the inset of Fig. 1, reflections 201, 011, 102, … , which are primitive reflections, are weak but still exist. Considering the atomic coordinates, it is obvious that the P Bravais lattice is essentially due to oxygen atoms since Bi and P atoms both occupy 4(*c*) *x*, 1/4, *z*, special positions with $z \approx 0$ for the former and $z \approx 0.5$ for the latter, involving a quasi-B sublattice. In the same way, the Zn(1) and Zn(2) atoms almost coincide by the 1/2, 0, 1/2 translation. Thus, the primitive Bravais lattice involves a slight tilt between the oxygen polyhedra surrounding the cations. This is evidenced in Fig. 4 by comparing the tunnels centered at the origin to the tunnel centered on 1/2, 0, 1/2. $BiZn_2PO_6$ and $BiCu_2PO_6$ are isostructural. This is common to all the materials of the series adopting the *Pnma* space group. The ionic radii of Cu^{2+} and Zn^{2+} in 5-coordination being close, 0.65 and 0.68 Å respectively (21), they keep the same

TABLE 1
Details of Rietveld Refinement for $BiZn_2PO_6$

Space group	*Pnma*
Cell dimensions (Å)	$a = 11.8941(3)$
	$b = 5.2754(2)$
	$c = 7.8161(2)$
Volume (Å^3)	490.44
Z	4
2θ range (°)	10–123
Step scan (°2θ)	0.02
Time/step (s)	40
Number of reflections	854
Number of refined parameters	44
Zero point (°2θ)	$-0.011(2)$
Background	modelled by points
Profile function	Pearson VII ($m = 0.94(3)$)
Profile parameters	$U = -0.005(3)$ $X = 0.0053(6)$
	$V = 0.038(2)$
	$W = -0.0005(2)$
Asymmetry	Asy1 $= -0.34(5)$
	Asy2 $= -0.11(3)$
	Asy3 $= 0.70(11)$
	Asy4 $= 0.25(6)$
$R_{wp} = \left[\sum_i w_i(y_i - y_{ci})^2 / \sum_i y_i^2\right]^{1/2}$	0.155
$R_p = \sum_i \lvert y_i - y_{ci}\rvert / \sum_i y_i$	0.124
$R_F = \sum_i \lvert\lvert F_{obs}\rvert - \lvert F_{cal}\rvert\rvert / \sum_i \lvert F_{obs}\rvert$	0.0380
$R_{Bragg} = \sum_k \lvert I_k - I_k^{cal}\rvert / \sum_k I_k$	0.0564
$\chi^2 = [R_{wp}/R_{exp}]^2$	4.49

pyramidal environment in the framework with almost identical distances (4). Therefore the $BiCu_2VO_6$ compound exhibits a supercell characterized by the *b* axis tripling and the symmetry lowering to monoclinic. In the latter, one third of the Cu^{2+} adopts an octahedral environment (8). The point symmetry of the phosphorus atom decreased from

TABLE 2
Atomic and Lp Coordinates for $BiZn_2PO_6$

Atom	Site	x	y	z	B_{eq} or B(Å^2)[a]
Bi	4*c*	0.0990(2)	1/4	0.0119(3)	1.1(2)
Zn(1)	4*c*	0.1028(7)	0.75	0.6915(6)	0.9(2)
Zn(2)	4*c*	0.0930(7)	0.75	0.3011(6)	0.5(2)
P	4*c*	0.1945(8)	1/4	0.481(2)	1.4(3)
O(1)	8*d*	−0.010(2)	−0.006(4)	0.191(2)	0.4(2)
O(2)	8*d*	0.123(1)	0.497(2)	0.489(3)	0.4(2)
O(3)	4*c*	0.285(1)	1/4	0.604(2)	0.4(2)
O(4)	4*c*	0.245(2)	1/4	0.315(3)	0.4(2)
Lp		0.171	0.25	0.012	

[a] $B_{eq} = \frac{4}{3}\sum_i\sum_j \beta_{ij} a_i a_j$.

TABLE 3
Selected Interatomic Distances (Å) and Bond Angles (°) for $BiZn_2PO_6$

Bismuth environment		Lp–O	Lp–Bi–O
Bi–Lp	0.85		
Bi–O(1)^{vi}	2.30(2)	2.795	117.34
Bi–O(1)^{viii}	2.30(2)	2.795	117.34
Bi–O(1)^{i}	2.34(2)	2.902	123.77
Bi–O(1)^{iii}	2.34(2)	2.902	123.77
Bi–O(4)^{viii}	2.94(2)	2.527	53.63
Bi–O(3)$^{ii}_{001}$	3.062(5)	2.784	63.23
Bi–O(3)$^{ii}_{011}$	3.062(5)	2.784	63.23
⟨Bi–O⟩	2.619		
$Zn(1)O_5$ environment			
Zn(1)–O(1)$^{vi}_{001}$	1.97(2)	O(1)$^{vi}_{001}$–Zn(1)–O(1)$^{viii}_{011}$	86(1)
Zn(1)–O(1)$^{viii}_{011}$	1.97(2)	O(1)$^{vi}_{001}$–Zn(1)–O(2)$^{iii}_{010}$	149(1) × 2
Zn(1)–O(2)	2.09(2)	O(1)$^{vi}_{001}$ − Zn(1)–O(2)	89(1) × 2
Zn(1)–O(2)$^{iii}_{010}$	2.09(2)	O(1)$^{v}_{011}$–Zn(1)–O(4)^{ii}	106(1) × 2
Zn(1)–O(4)^{ii}	2.05(2)	O(2)^{i}–Zn(1)–O(2)$^{iii}_{010}$	80(1)
⟨Zn(1)–O⟩	2.034	O(2)^{i}–Zn(1)–O(4)^{ii}	105(1) × 2
$Zn(2)O_5$ environment			
Zn(2)–O(1)$^{i}_{010}$	1.98(2)	O(1)$^{i}_{010}$–Zn(2)–O(1)^{iii}	81(1)
Zn(2)–O(1)^{iii}	1.98(2)	O(1)$^{i}_{010}$–Zn(2)–O(2)^{i}	149(1) × 2
Zn(2)–O(2)^{i}	2.02(2)	O(1)$^{i}_{010}$–Zn(2)–O(2)$^{iii}_{010}$	90(1) × 2
Zn(2)–O(2)$^{iii}_{010}$	2.02(2)	O(1)^{vi}–Zn(2)–O(3)$^{ii}_{001}$	96(1) × 2
Zn(2)–O(3)$^{ii}_{001}$	2.12(2)	O(2)^{i}–Zn(2)–O(2)$^{iii}_{010}$	83(1)
		O(2)^{i} − Zn(2)–O(3)$^{ii}_{001}$	114(1) × 2
⟨Zn(2)–O⟩	2.024		
PO_4 tetrahedron			
P–O(2)^{i}	1.56(1)	O(2)^{i}–P–O(2)^{iii}	114(1)
P–O(2)^{iii}	1.56(1)	O(2)^{i}–P–O(3)^{i}	112(1)
P–O(3)^{i}	1.44(2)	O(2)^{i}–P–O(4)^{i}	105(1)
P–O(4)^{i}	1.43(3)	O(2)^{iii}–P–O(3)^{i}	112(1)
		O(2)^{iii}–P–O(4)^{i}	105(1)
⟨P–O⟩	1.50	O(3)^{i}–P–O(4)^{i}	107(1)
		⟨O–P–O⟩	109

Note. i: x, y, z. ii: $\frac{1}{2}-x, \frac{1}{2}+y, \frac{1}{2}+z$. iii: $x, \frac{1}{2}-y, z$. iv: $\frac{1}{2}-x, -y, \frac{1}{2}+z$. v: $\frac{1}{2}+x, y, \frac{1}{2}-z$. vi: $-x, \frac{1}{2}+y, -z$. vii: $\frac{1}{2}+x, \frac{1}{2}-y, \frac{1}{2}-z$. viii: $-x, -y, -z$.

2*mm* for $BiMg_2PO_6$ and $BiCd_2PO_6$ (space group *Bbmm*) to *m* in $BiZn_2PO_6$. It results in a more distorted tetrahedron and in a tilt of about 8° around *b* between the two

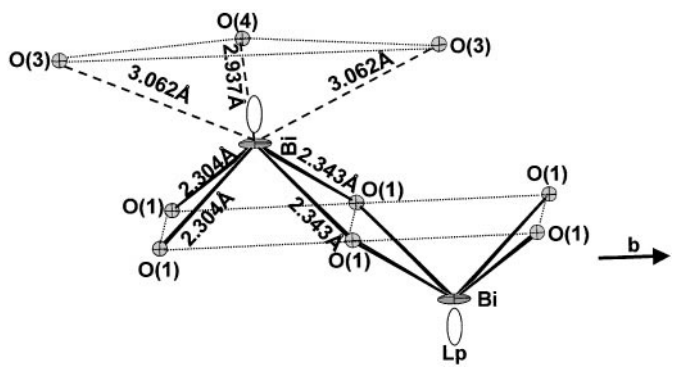

FIG. 2. Bismuth environment evidencing the lone pair position (Lp). $[BiO_2]^-$ chains are running along the *b* axis.

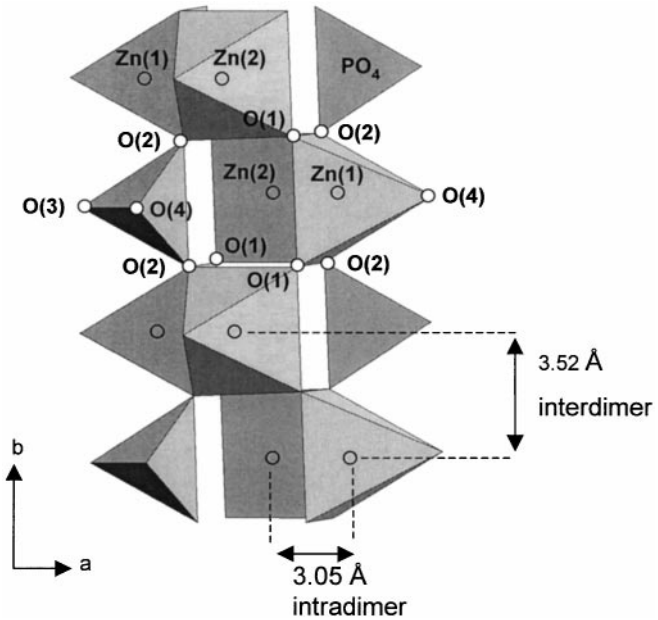

FIG. 3. $[ZnO_3^{4-}]_\infty$ columns and bidentate phosphate groups.

TABLE 4
Orthorhombic Unit Cell Parameters, Space Group and M^{2+} Ionic Radius for BiM_2XO_6 Compounds at Room Temperature

Compound	a (Å)	b (Å)	c (Å)	Space group	Ionic radius for M^{2+} (coord)[a]
$BiCu_2PO_6$	11.776(1)	5.1730(6)	7.7903(6)	*Pnma*	0.65 (V)
$BiMg_2PO_6$	11.888(3)	5.273(2)	7.801(2)	*Bbmm*	0.66 (V)
$BiMg_2VO_6$	12.246(2)	5.444(2)	7.9136(6)	*Pnma*	0.66 (V)
$BiMg_2AsO_6$	12.1637( )	5.3898(4)	7.9142(5)	*Bbmm*	0.66 (V)
$BiCd_2PO_6$	11.944(2)	5.3740(2)	8.5050(8)	*Bbmm*	0.87 (V)
$BiPb_2PO_6$	11.473(6)	5.930(4)	9.079(10)	*Pbnm*	1.19 (VI)
$BiCa_2PO_6$	11.950(2)	5.542(1)	8.891(1)	$Bb2_1m$	1.00 (VI)
$BiCu_2VO_6$[b]	12.401(3)	5.261(1)	7.824(2)	—	0.65 (V)
$BiCu_2AsO_6$	12.253(1)	5.280(1)	7.577(1)	*Pnma*	0.65 (V)
$BiZn_2PO_6$	11.8941(3)	5.2754(2)	7.8161(2)	*Pnma*	0.68 (V)

Note. [a]From Ref. (21). [b]Ref. (8) gives the $a = 13.4932(1)$, $b = 7.8224(1)$, $c = 15.7972(1)$, $\beta = 113.11(1)^\circ$ monoclinic unit cell, considering additional reflections.

[b]The unit cell was initially refined from fundamental reflections with in the orthorhombic lattice (11).

structural types. The tilt is clearly observable in Figs. 4 and 5, through the perfectly rectangular channel sections for $BiMg_2PO_6$. The Mg–O distances remain nearly unchanged (2×2.04, 2×2.07 and 1.94 Å) since its ionic radius is close, 0.66 Å. Therefore, Cd–O distances drastically increase to 2×2.20, 2×2.14, and 2.31 Å in relation with the greatest cationic size, $r_{Cd^{2+}} = 0.87$ Å (5). For $BiCu_2PO_6$, the square pyramidal coordination of copper to oxygen atoms is very

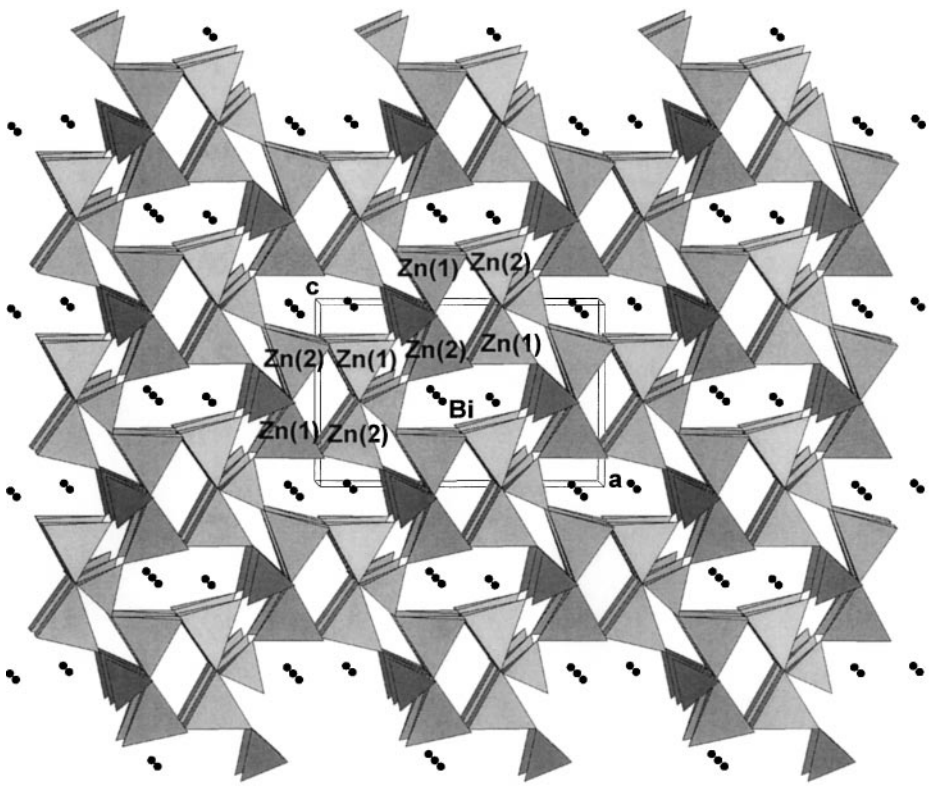

FIG. 4. Projection along the b axis of the $BiZn_2PO_6$ crystal structure.

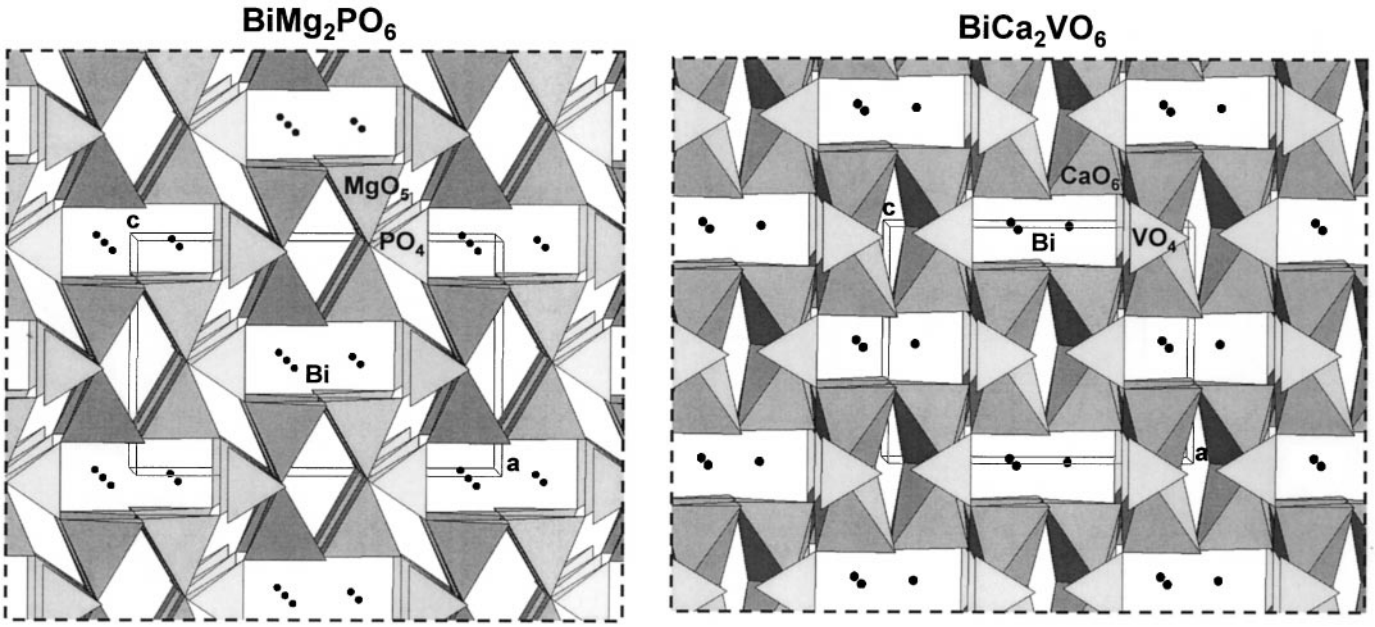

FIG. 5. Comparison between $BiMg_2PO_6$ and $BiCa_2VO_6$ structures viewed along the *c* axis.

distorted with four bonds to the basal oxygens at about 1.94–2.02 Å and one to the apical oxygen at about 2.19 Å. In fact, the copper coordination is rather 4 + 1; such a coordination is currently observed for a copper atom. The Jahn Teller effect distorts the octahedral coordination with two longer apical Cu–O bonds, leading to 4 + 1 + 1 coordinations; one of the two apical oxygen atom is sometimes at a distance from copper higher than 3 Å. The distancing of the apical O(4) atom from the copper atom has two effects: (i) the PO_4 tetrahedron is more rotated around *b* (about 14°) and (ii) the O(4) atom is brought nearer to the Bi atom, and must be considered as belonging to the Bi coordination polyhedron. Such a 5-coordination of bismuth is found, for example, in the Aurivilius phases. The case of $BiCa_2VO_6$ gets more complex, rule by the acentric $Bb2_1m$ space group in the chosen orientation. Eventually, this material was considered as ferroelectric with electric moments switchable by a PO_4^{3-} rotation with the polar axis being *c*. The centric $BiMg_2XO_6$ might then be regarded as its paraelectric form. The oxygen coordination around Ca^{2+} is probably related to its larger size, $r_{Ca^{2+}} = 1.0$ Å. Six oxygen atoms form a distorted octahedron with Ca–O ionic bonds ranging from 2.28 to 2.62 Å (3). Thus, two octahedra share their O(2)–O(3) edge to form dimers that connect to each other by the O(1) corners as shown in Fig. 6. The obtained double columns have the $[CaO_4^{6-}]_\infty$ formula instead of $[MO_3^{4-}]_\infty$ for MO_5 primary bricks. Two fundamental changes are then observed: (1) there is a strong tilt of PO_4^{3-} groups that have a O_3 face parallel to the (*a*, *c*) plane, and (2) the columns are not independent anymore but are gathered to four other columns by common O(1)O(4)O(4) faces. It is noteworthy that within the columns a seventh Ca–O(3) distance of 2.78 Å appears that was not considered to simplify the

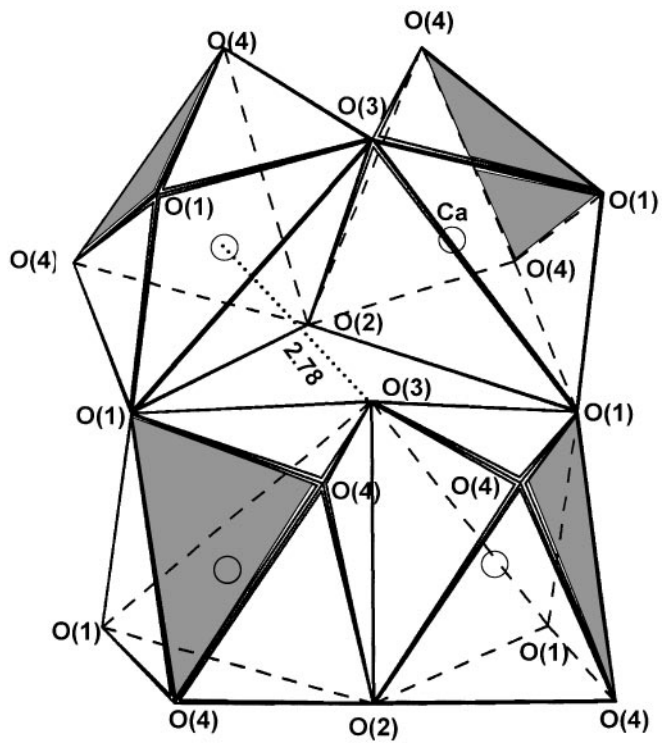

FIG. 6. Connection between two Ca_2O_{10} dimers in $BiCa_2VO_6$. The connections between columns are assured by the O(1)O(4)O(4) dark sides.

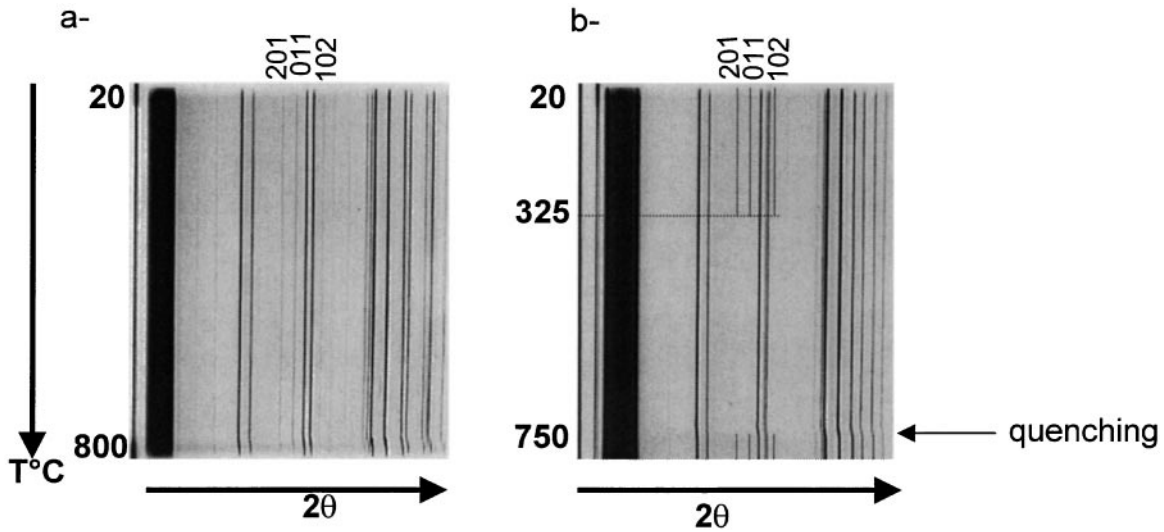

FIG. 7. High-temperature X-ray diffraction pattern of (a) $BiCu_2PO_6$ and (b) $BiZn_2PO_6$. In this pattern the extra lines have been darkened for clarity.

description. Finally, $BiPb_2PO_6$ crystal structure was refined in the *Pbnm* space group. Probably because of the additional disorder effect due to Pb^{2+} $6s^2$ lone pair and of the strongly distorted PbO_6 octahedron, two configurations of the PO_4 tetrahedra coexist in the framework (6).

Recently by refinement of the data collections performed in the range 100 K to 350 K, Radosavljevic *et al.* showed a primitive orthorhombic unit cell at room temperature for $BiMg_2VO_6$ (12), whereas it is base centered at 350 K. X-ray powder diffraction spectra versus temperature were obtained with a Guinier–Lenné focusing camera for $BiCu_2PO_6$ and $BiZn_2PO_6$ which adopt primitive orthorhombic cell at room temperature (Fig. 7). The *hkl* reflections with $h + l = 2n + 1$ (201, 011, and 102) are progressively weakened and disappear at about 325°C for $BiZn_2PO_6$. Therefore, $BiZn_2PO_6$ undergoes a $P \rightarrow B$ transition at 325°C. After quenching, the extra reflections quickly reappear, involving a totally reversible transition. As discussed above, such a transition mainly involves the rotation of PO_4 tetrahedra involving a more regular ZnO_5 polyhedron; so far, this low-energy displacive transition could not be detected by DSC nor by DTA experiment. The unit cell parameters refined at 700°C are $a = 11.9576(3)$ Å, $b = 5.3016(1)$ Å, $c = 7.8479(2)$ Å and confirm the expected unit cell expansion. For $BiCu_2PO_6$, the no-*B* reflections remain from 20 to 800°C, and the *P*-to-*B* transition could take place at higher temperature in accordance with the higher value of the tilt angle of the PO_4 tetrahedra (14°). It also may not arise due to the already discussed Jahn–Teller effect that stabilizes a strongly distorted oxygen polyhedron around Cu^{2+}.

REFERENCES

1. J. Huang and A. W. Sleight, *J. Solid State Chem.* **100,** 170 (1992).
2. J. Huang, Q. Gu, and A. W. Sleight, *J. Solid State Chem.* **105,** 599 (1993).
3. I. Radosavljevic, J. S. O. Evans, and A. W. Sleight, *J. Solid State Chem.* **137,** 143 (1998).
4. F. Abraham, M. Ketatni, G. Mairesse, and B. Mernari, *Eur. J. Solid State Chem.* **31,** 313 (1994).
5. N. Tancret, Ph.D. dissertation, Université des Sciences et Technologies de Lille, France, September 1995.
6. A. Mizrahi, J. P. Wignacourt, and H. Steinfink, *J. Solid State Chem.* **133,** 516 (1997).
7. A. Mizrahi, J. P. Wignacourt, M. Drache, and P. Conflant, *J. Mater. Chem.* **5,** 901 (1995).
8. I. Radosavljevic, J. S. O. Evans, and A. W. Sleight, *J. Solid State Chem.* **141,** 149 (1998).
9. M. Ouchabi, F. Kzaiber, M. Diouri, M. Agunaou, A. Sadel, and B. Mernari, Proceeding on the VIIIth REMCES, Tetouan, Morocco, 1999.
10. I. Radosavljevic, J. S. O. Evans, and A. W. Sleight, *J. Alloys Compd.* **284,** 99 (1999).
11. M. Ketatni, Ph.D. dissertation, Université des Sciences et Technologies de Lille, France, April 1995.
12. I. Radosavljevic and A. W. Sleight, *J. Solid State Chem.* **149,** 143 (2000).
13. A. W. Visser, *J. Appl. Crystallogr.* **2,** 89 (1969).
14. G. S. Smith and R. L. Snyder, *J. Appl. Crystallogr.* **12,** 60 (1979).
15. J. Rodriguez-Carjaval, Fullproof 98, Laboratoire Leon Brillouin, CEA-CNRS, France, 1998.
16. J. Galy and R. Enjalbert, *J. Solid State Chem.* **44,** 1 (1982).
17. A. Verbaere, R. Marchand, and M. Tournoux, *J. Solid State Chem.* **23,** 383 (1978).
18. P. P. Ewald, *Ann. Phys.* **64,** 253 (1921).
19. E. Morin, G. Wallez, S. Jaulmes, J. Couturier, and M. Quarton, *J. Solid State Chem.* **137,** 283 (1998).
20. R. D. Shannon, *J. Appl. Phys.* **73,** 348 (1993).
21. R. D. Shannon, *Acta Crystallogr. A* **32,** 751 (1976).